EUROFUSION WPJET4-CP(16) 15273

F Durodie et al.

ITER-like antenna for JET first results of the advanced matching control algorithms

Preprint of Paper to be submitted for publication in Proceedings of 29th Symposium on Fusion Technology (SOFT 2016)

This work has been carried out within the framework of the EUROfusion Consortium and has received funding from the Euratom research and training programme 2014-2018 under grant agreement No 633053. The views and opinions expressed herein do not necessarily reflect those of the European Commission.

ITER-like antenna for JET first results of the advanced matching control algorithms

F. Durodié[a], P. Dumortier[a,1], T. Blackman[b], E. Wooldridge[b], E. Lerche[a,b], W. Helou[c], R.H. Goulding[d], M. Kaufman[d], D. Van Eester[a], M. Graham[b], E. Wooldridge[b], JET Contributors[1]

[a]*LPP-ERM/KMS, TEC Partner, Brussels, Belgium*
[b]*CCFE, Culham Science Centre, Abingdon, OX14 3DB, UK*
[c]*CEA, IRFM, F-13108 St-Paul-Lez-Durance, France*
[d]*Oak Ridge National Laboratory, PO Box 2008, Oak Ridge, United States*

Abstract

The ITER-like Antenna (ILA) [1] for JET is a 2 toroidal by 2 poloidal array of Resonant Double Loops (RDL). It features in-vessel matching capacitors feeding RF current straps in Conjugate-T (CT) manner, a low impedance quarter-wave impedance transformer and a service stub allowing hydraulic actuator and water cooling services to reach the aforementioned capacitors. A Second Stage Matching (SSM) trombone and stub circuit allows to match the chosen conjugate-T working impedance to 30Ω. Toroidally adjacent RDLs are fed from a 3dB hybrid splitter.

The assessment of the ILA results (2008-9) identified that achieving routine full array operation required a better understanding of the RF circuit, tighter calibrations of RF measurements and last but not least a feedback control algorithm for the SSM.

The matching and phasing of the array is controlled by 22 feedback loops actuating the 8 matching capacitors, the 4 second stage trombones and 4 stubs, the 4 Main Transmission Line (MTL) phase shifters and the 4 phases with respect to a reference of the generators feeding the upper and lower half array through 3dB hybrid combiner-splitters.

The circuit was extensively simulated [2] allowing the development of an algorithm to drives the SSM circuit components, trombone and stub, to optimal locations with respect to the measured remaining VSWR excursions due to ELMs.

The paper focusses on the new additional matching algorithms and assesses their performance.

Keywords: ICRH, Matching, Control

1. Introduction

The achievements of the ILA for the 2008-9 experimental campaigns are reviewed in [1] and [3] also reviews the achievements up to date for the presently refurbished ILA.

The major improvements required to make the ILA usable for the JET programme were assessed. First, the implementation of a feedback control of the Second Stage Matching (SSM) matching circuit which compensates the residual mismatch left by the fixed quarter wave (at 42 MHz) in-vessel impedance transformer for the chosen Conjugate-T (CT) point impedance. Secondly, it was noticed that in order to adequately control the ILA array it was necessary to improve on the quality of the calibration of the RF signals.

Finally, the ILA suffers from the fact that the 2 straps constituting an RDL are asymmetric which adversely affect the load tolerant properties of the low impedance CT operation. Although this was partially acknowledged during the design phase of the ILA no other satisfactory geometric solution was found to alleviate this issue within the boundaries of the ILA project. Therefore, in order the improve the load tolerance of the ILA as much as possible the algorithm setting the SSM components was designed to offset the matching automatically in the presence of ELMs.

As a result the 4 RDLs making up the ILA total 24 RF actuators (assuming equal powers feeding each RDL) which are controlled by 22 feedback loops (19 independent loops) which are shown in Figure 1. The feedback controlled quantities are 4 complex CT impedances controlled by the 8 in-vessel capacitors, 4 complex MTL reflection coefficients controlled by the 4 SSM trombones and stubs, 2 toroidal phases between straps 2 and 6 and between straps 3 and 7 controlled by the 4 MTL phase shifters, the poloidal phase difference between either strap 2, strap 6 or an average of these and a reference phase for the ILA upper half array and similarly for the lower half array controlled by a combination of the 4 RF amplifier output phases (taking into account the correct phase inputs to the 3dB combiners).

2. Matching Algorithms

2.1. Conjugate T-point Impedance

The algorithm for the control of the Conjugate T-point (CT) impedance, Z_{CT}, was not modified from the 2008-2009 experimental campaigns [4]. Its implementation is now using FPGA technology based on National Intruments / Labview [5] instead of the general purpose CPU module running Labview code.

[1] See the Appendix of F. Romanelli et al., Proceedings of the 25th IAEA Fusion Energy Conference 2014, Saint Petersburg, Russia

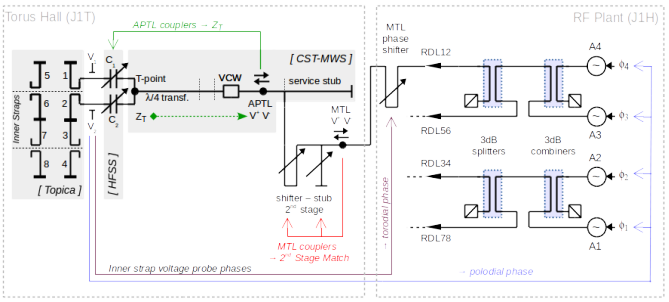

Figure 1: Schematic view of the circuit model showing the ILA strap array, the components of RDL_{12}, the "3dB" hybrid splitters and combiners and RF sources feeding the top and bottom RDLs as well as the various feedback loops.

The CT impedance for an RDL is estimated from the Antenna Pressurized Transmission Line (APTL) forward and reflected Directional Coupler (DC) signals. The calibrated DC forward, V_f, and reflected, V_r, signals are found from the raw amplitude and phase signals, m_f, Φ_f, m_r and Φ_r by subtracting amplitude offsets Δm_f and Δm_r and application of the directional coupler's calibration matrix, $\mathbf{C}$. A coefficient matrix, $\mathbf{T}$, transforms the calibrated forward and reflected voltage waves into the CT RF voltage, V_{ct}, and current, I_{ct} from which then Z_{ct} is computed).

$$Z_{ct} = \frac{V_{ct}}{I_{ct}} \quad \text{with} \quad \begin{bmatrix} V_{ct} \\ I_{ct} \end{bmatrix} = \mathbf{T} \cdot \begin{bmatrix} V_f \\ V_r \end{bmatrix} = \underbrace{\mathbf{T} \cdot \mathbf{C}}_{\mathbf{K}} \cdot \begin{bmatrix} (m_f - \Delta m_f) e^{j\Phi_f} \\ (m_r - \Delta m_r) e^{j\Phi_r} \end{bmatrix} \tag{1}$$

Different from 2008-9 when the transformation was done using a series of transmission line sections, $\mathbf{T}$ is now found from a Microwave Studio [6] model of the APTL with the Vacuum Ceramic Window (VCW), bellows and the transition between the 30Ω circular feed and the low impedance quarter wave transformer's rectangular cross-section. Matrices $\mathbf{T}$ and $\mathbf{C}$ are combined into one matrix $\mathbf{K}$ for the implementation.

The error signals for the top and bottom capacitors, resp. $\mathcal{E}_t$ and $\mathcal{E}_b$, for a given target CT impedance Z_M are found as before:

$$\mathcal{E}_t = \pm Re\left[e^{\alpha}\frac{Z_M}{Z_{ct}} - y_M\right] \quad \text{and} \quad \mathcal{E}_b = Im\left[e^{\alpha}\frac{Z_M}{Z_{ct}} - y_M\right] \tag{2}$$

Where the sign of $\mathcal{E}_t$ depends on the chosen matching solution, α is a rotation angle basically depending on the local topology of Z_{ct} in the vicinity of the target Z_M in the C_t, C_b plane and y_M is an offset admittance that was introduced in the 2008-9 algorithm to offset the match for the ELMs: it was kept but it is set to $1 + 0j$.

The capacitor's error is scaled by a factor $Q_{c,k}$ with $k = t$ or b depending on the normalized capacitor voltage, $U_{c,k}$, which will slow down the capacitor movement near a resonance when the capacitor voltage, $V_{c,k}$ is high:

$$Q_{c,k} = \frac{P_k}{1 + \left(\frac{U_{c,k}}{V_{ref}}\right)^{V_{exp}}} \quad \text{with} \quad U_{c,k} = \frac{V_{c,k}}{\sqrt{max\left(V_f^2 - V_r^2, V_{thr}^2\right)}} \tag{3}$$

Where P_k, V_{ref} and V_{exp} are adequately chosen constants: typically P_k =10 (max) for the capacitors of the powered RDLs and 0 for the others, V_{ref} =3.5 and V_{exp} =3. V_{thr} is to avoid a singularity (or negative) when computing $U_{c,k}$ when the (APTL) transmitted power is too low and is typically 50.

The capacitor corrections are then clipped against a maximum allowed correction per time cycle, ΔC_{max}:

$$C_k \leftarrow C_k + min\left(max\left(-\Delta C_{max},\ Q_{c,k} \cdot \mathcal{E}_k\right), +\Delta C_{max}\right) \tag{4}$$

Another change is that the algorithm's cycle time is not fixed as it was with the earlier implementation to ≈5ms but is dependent on the RF pulse length such that ≈2000 measurements are recorded. As a consequence the behaviour of the algorithm depends (slightly) on the pulse length by being a bit slower to home in to the match for longer pulses.

2.2. 2^{nd} Stage Main Transmission Line VSWR

The algorithm works on 2 time scales. On the 2μs cycle time scale of the Amplitude and Phase Demodulator Module (APDM) which processes the RF signals, a time scale fast enough to resolve the RF coupling variations due to ELM transitions, the reflection coefficients in the MTLs are recorded in a relatively crude polar map of typically 8 phase bins and 15-20 amplitude bins (see Figure 2(b)). The recording is done by filling an integer, N, proportional to the tracking time interval the algorithm should consider: $N = tracking\ time/fast\ cycle\ time$. At each fast cycle the non-zero elements of the map are decremented by one.

On a slower time scale of ≈2000 samples for the RF pulse length (≈5ms for a 10s pulse) the average reflection coefficient is estimated from (remaining) non-zero entries in the polar reflection coefficient map, and the normalized admittance, y_{MTL} at the MTL side of SSM stub is found. The error signals for the SSM trombone, $\mathcal{E}_{Tr}$, and stub, $\mathcal{E}_{St}$, are then computed as:

$$\mathcal{E}_{Tr} = \pm\, k_G \cdot Re\left[y_{MTL} - 1\right] \quad \text{and} \quad \mathcal{E}_{St} = k_B \cdot Im\left[y_{MTL}\right] \tag{5}$$

The sign of $\mathcal{E}_{Tr}$ depends on the choice of the matching solution for the SSM (capacitive or inductive reactance for the SSM stub) in order to find a solution within the range of the SSM stub and trombone.

These error signals are then translated into 3 digital outputs controlling the movements of the SSM stub and trombone: ***move*** will be true when the error signal is above a certain threshold value, ***direction*** depends on the sign of the error signal and ***fast*** will be true if the signal exceeds a certain value and will cause the component to move at the fast pace (165mm/s for the trombone and 50mm/s for the stub) rather than the slow one (resp. 16mm/s and 10mm/s).

The algorithm was simulated extensively [2] and found stable with respect to the CT impedance algorithm and the toroidal phase controlled by the MTL phase shifters.

The effect of the action of the SSM algorithm during an RF pulse is shown in Figure 2 for the selected pulse JPN 89911 powering the lower half of the ILA array with about 500kW at 42MHz for a CT target impedance of 10-5j Ω with an algorithm tracking time of about 128ms (N=64000 (max)). The reflection coefficient maps shown in Figure 2(b) have been reconstructed

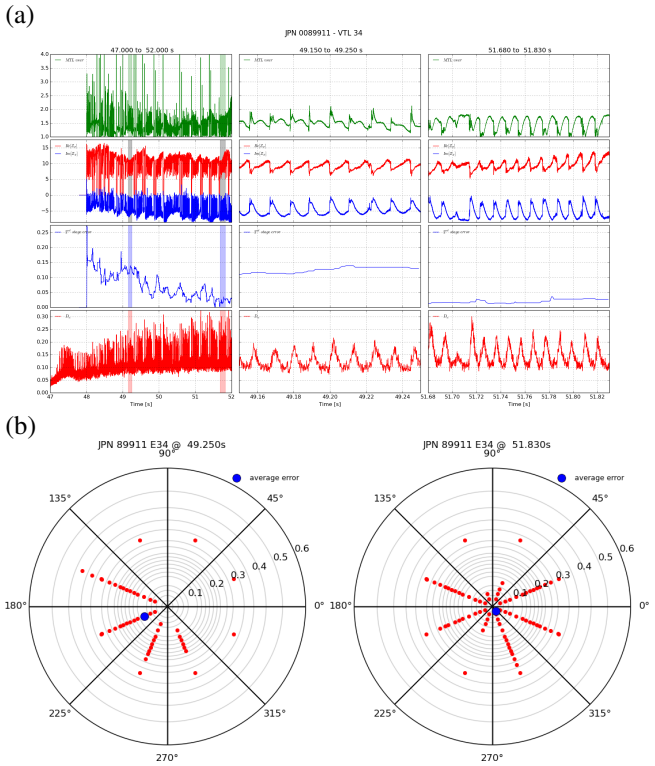

Figure 2: (a) Initial ELMy H-mode phase of JPN 89911 shown for RDL of straps 3 and 4. 1^{st} row: MTL VSWR, 2^{nd} row: CT- impedance, 3^{rd} row: SSM algorithm average MTL reflection coefficient and 4^{th} row: the D_α light emmission signal evidencing the ELMs. The 1^{st} column gives the overview of this phase indicating the the time intervals where the signals were expanded in the 2^{nd} and 3^{rd} column. (b) The SSM algorithm reflection coefficient maps for the two expanded time intervals shown above. The maps clearly show the used amplitude and phase bins as well as the averaged reflection coefficient.

from the fast data acquisition RF signals with a sample time of 5μs instead of the 2μs cycle time as the algorithm's FPGA internal fast data as well as the maps are not recorded. Consequently, N=128ms/5μs=25600 was used to process the signals for the figure instead. Unfortunately, at present, although the SSM stub and trombone digital inputs are recorded, the actual movements are not.

One can clearly see the average reflection coefficient decreasing while the shape of the MTL VSWR signals responding to ELMs transforms to actually decreasing during ELMs.

On stationary L-mode plasmas it is observed that the SSM algorithm reduces the MTL VSWR to below 1.2-1.3 when the SSM matching solution is in range of the SSM stub and trombones which is the case for frequencies above 33MHz and which more or less shows the present overall accuracy of SSM algorithm taking into account calibrations and dead bands.

2.3. Phase control

The phasing of the ILA array is measured on the voltage probes of "inner" straps (numbers 2, 3, 6 and 7) which have the highest (poloidal) cross-coupling with each other.

The phase difference between toroidally adjacent RDLs is controlled by the phase shifter trombones located in each of the 4 Main Transmission lines (MTL) in the RF plant building (J1H). As with the SSM stubs and trombones, there is a dead band and a switch over point between slow and fast movement of the trombones.

The poloidal phase control is done for the upper and lower ILA array halves each with respect to a separate phase reference driving the 4 amplifier output phases taking into account the extra condition of the phasing at the 3dB combiners. The algorithm has presently some issues related to the phase roll-overs occurring at $\pm\pi$ which required a manual set up of the reference phases in order to avoid those.

Figure 3 shows the inner strap phase differences for JPN 90924. This is a full ILA array on an ELMy H-mode plasma fully controlled by all algorithms at a power level of 1.2MW doubling the power of JPN 76769 of the 2009 campaign.

Unfortunately further progress was not possible due to issues appearing on RDL56. These were initially identified as CT-point arcs but later turned out to be the consequence of an hydraulic fluid leak sadly terminating the operation of the ILA upper half array for next foreseeable future.

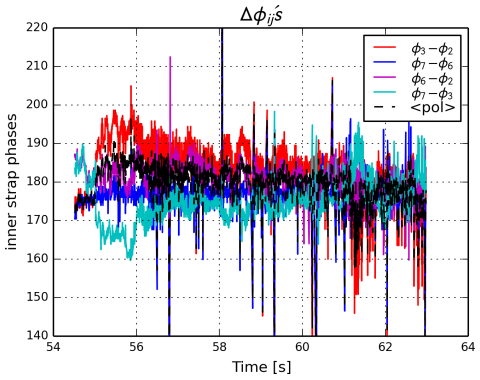

Figure 3: Inner strap phases for JPN 90924.

3. Experiment vs Simulation

In order to compare the experiment with the simulation [2] the measured RF signals are averaged over a small stationary phase of an L-mode discharge. The simulator uses the power fed to the active RDLs, the capacitor values of all RDLs as well as a set of Topica [7] matrices as parameters to best fit the capacitor voltages, the complex APTL directional coupler voltages and the amplitudes of the MTL directional coupler voltages. The resulting fit for JPN 89652 with a Radial Outer Gap (ROG: a measure for the distance between the ILA and the plasma) of 5cm is shown in Figure 4 where as the comparison between the fitting capacitor values and CT impedances with the measured ones are shown in Figure 5. It is worth noting that for this pulse only the lower ILA array half was powered and that the cross-coupled voltages on the upper half were quite accurately reproduced. Finally the residue of the fitting process vs. the best fitting Topica matrix (ordered and interpolated along the distance between the antenna to the plasma parameter (but with an arbitrary offset)) is shown in Figure 6 for JPN 89652 and JPN 89653 with a ROG of 7cm. The fitting of both

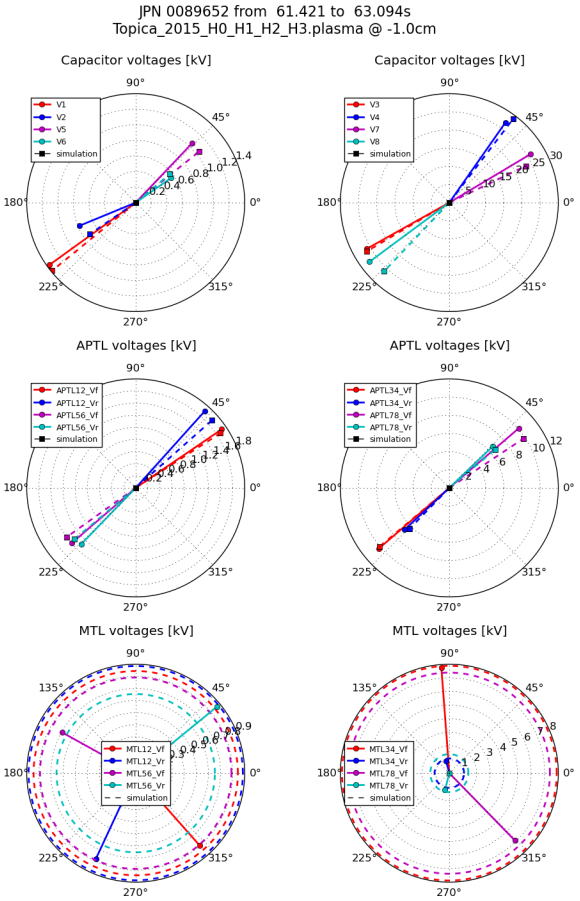

Figure 4: The comparison of the RF voltages between the measured signals and the ones fitted by simulation: (left) unpowered upper half ILA array (right) powered lower half ILA array. (top) capacitor voltages (middle) APTL directional coupler voltages (bottom) MTL directional coupler signals (only amplitudes of the simulation/fit are shown

pulses shows that the difference in antenna to plasma distance is accurately estimated by the modelling in the fitting process.

4. Conclusions

The implementation of the SSM algorithm has significantly improved the operational ease of the ILA. The algorithm finds the optimum location of SSM stub and trombone for the measured range of VSWR variations measured during the past observation time interval despite the fact that the real VSWR transients due to ELMs is far more complex than those simulated. At present the maximum tracking time interval is limited to a maximum of 128ms which maybe slightly too short if the ELM frequency is low.

The CT impedance algorithm's new implementation as well as the more thorough calibration appears to be much more stable than the previous implementation and has lead to successfully operate the ILA at a much wider range of frequencies (29-51MHz for the upper half and 29-49MHz for the lower one). The response time of the CT impedance matching loop is dependent on the RF pulse length and a future modification is planned in order to further decrease its response time.

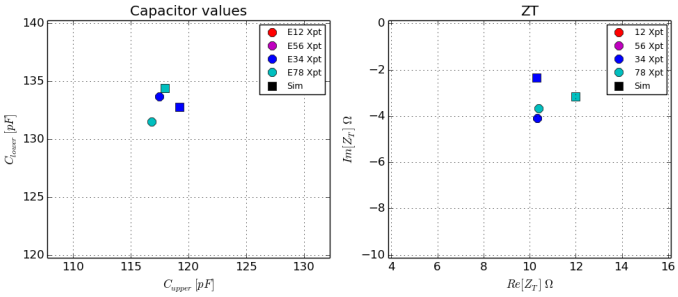

Figure 5: (left) measured vs fitted capacitor values for the lower half ILA array (right) measured vs fitted CT impedances

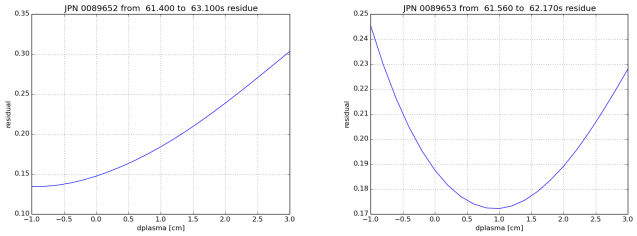

Figure 6: The residue vs the selected Topica ILA array input impedance matrix best fitting the RF voltages for (left) JPN 89652 with a ROG of 5cm and (right) JPN 89653 with an ROG of 7cm

It is worth noting that the modelling of the ILA is presently able to rather accurately reproduce experimental results.

There has been limited full array operation on plasmas due to a number of technical issues in part not related to the algorithms' performance. The few pulses done show that the full array control on moderately ELMy H-mode plasmas is possible and that the ILA had become usable in experimental campaigns.

It is thus very unfortunate that the ILA upper half array is now inoperable.

Acknowledgements: *This work has been carried out within the framework of the EUROfusion Consortium and has received funding from the Euratom research and training programme 2014-2018 under grant agreement No 633053. The views and opinions expressed herein do not necessarily reflect those of the European Commission.*

References

[1] F. Durodié *et al.*, Physics and engineering results obtained with the ion cyclotron range of frequencies ITER-like antenna on JET, Plasma Physics and Controlled Fusion 54 (7) (2012) 074012+. doi:10.1088/0741-3335/54/7/074012.
URL `http://dx.doi.org/10.1088/0741-3335/54/7/074012`

[2] F. Durodié *et al.*, Circuit Model of the ITER-like Antenna for JET and Simulation of its Control Algorithms, Proc. 20 th Top. Conf on RF power in Plasmas, AIP Conf. Proc. 1689, 070013 (2015)doi:10.1063/1.4936520.

[3] P. Dumortier *et al.*, Commissioning and first results of the reinstated JET ICRF ILA, this conference.

[4] M. Vrancken *et al.*, Proc. 17 th Top. Conf on RF power in Plasmas, AIP Conf. Proc. 933 (2007) 135.

[5] National instruments / labview, `http://www.ni.com/labview/`.

[6] CST GmbH, CST Microwave Studio®, User Manual (2014).

[7] V. Lancellotti *et al.*, TOPICA: an Accurate and Efficient Numerical Tool for Analysis and Design of ICRF Antennas, Nuclear Fusion 46 (2006) S476 – S499.